Time dependent evolution of vacancies and metallic domains and their correlation with the photochromic effect in yttrium oxyhydride films revealed by in situ illumination positron annihilation lifetime spectroscopy

Wu, Ziying; Chaykina, Diana; Schreuders, Herman; Schut, Henk; De Boer, Martijn; Liedke, Maciej Oskar; Brück, Ekkes; Dam, Bernard; Eijt, Stephan W.H.; More Authors

DOI
10.1103/PhysRevMaterials.9.015201

Publication date
2025

Document Version
Final published version

Published in
Physical Review Materials

Time dependent evolution of vacancies and metallic domains and their correlation with the photochromic effect in yttrium oxyhydride films revealed by *in situ* illumination positron annihilation lifetime spectroscopy

Ziying Wu [1,*] Diana Chaykina [1,2] Herman Schreuders [2] Henk Schut [3] Martijn de Boer,[3] Maciej Oskar Liedke [4] Maik Butterling [4] Andreas Wagner,[4] Marcel Dickmann,[5] Ekkes Brück [1] Bernard Dam [2] and Stephan W. H. Eijt [1]

[1]*Fundamental Aspects of Materials and Energy, Department of Radiation Science and Technology, Faculty of Applied Sciences, Delft University of Technology, Mekelweg 15, NL-2629 JB Delft, The Netherlands*

[2]*Materials for Energy Conversion and Storage, Department of Chemical Engineering, Faculty of Applied Sciences, Delft University of Technology, Van der Maasweg 9, NL-2629 HZ Delft, The Netherlands*

[3]*Neutron and Positron Methods for Materials, Department of Radiation Science and Technology, Faculty of Applied Sciences, Delft University of Technology, Mekelweg 15, NL-2629 JB Delft, The Netherlands*

[4]*Institute of Radiation Physics, Helmholtz-Zentrum Dresden-Rossendorf, Bautzner Landstrasse 400, D-01328 Dresden, Germany*

[5]*Institut für angewandte Physik und Messtechnik, Bundeswehr Universität München, D-85579 Neubiberg, Germany*

(Received 17 October 2024; accepted 6 January 2025; published 16 January 2025)

Grasping (electronic) structure changes during photochromic processes is crucial for fully understanding the photochromic effect in rare-earth oxyhydride films. In this study, we employ *in situ* UV illumination positron annihilation lifetime spectroscopy (PALS) to investigate the time evolution of open-volume defects and metallic domains during photodarkening and bleaching in yttrium oxyhydride films. The PALS depth profiles before and after a photodarkening-bleaching cycle reveal a light-induced increase in open-volume defects, that occurs homogeneously throughout the oxyhydride layer. The time-dependent PALS measurements show that upon photodarkening, a fast initial formation of metallic domains occurs, as well as a fast release of loosely bounded hydrogen from vacancy clusters and nanopores. During further photodarkening, the concentration of divacancy-like defects gradually increases due to the aggregation of light-induced hydrogen vacancies with preexisting yttrium monovacancies. After the UV illumination is stopped, two subsequent bleaching phases are observed. During the first bleaching phase, a strong correlation between the shortest positron lifetime τ_1 and the photochromic contrast is seen in both samples, suggesting that metallic domains disappear and, correspondingly, positron trapping at yttrium monovacancies and divacancy-like defects increases. During the second bleaching phase, a subsequent correlation between τ_1 and the photochromic contrast is observed in the more H-rich sample, which is related to the disappearance of larger metallic domains. After bleaching, most of the metallic domains and the photoexcited electrons in the matrix have disappeared, while the formed small vacancy complexes and larger vacancies remain stable. Our PALS study suggests that the formation of metallic domains is the cause of photodarkening, and the formed vacancy defects are important for understanding the memory effect.

DOI: 10.1103/PhysRevMaterials.9.015201

I. INTRODUCTION

Yttrium oxyhydride (YH_xO_y) thin films have attained increasing attention because of their color-neutral photochromic effect at ambient conditions, since the first report of the photochromism in yttrium oxyhydride thin films in 2011 [1]. YH_xO_y films are transparent semiconductors, but they can be darkened when subjected to photons with above-bandgap energies, causing a reduction in the transmittance in a broad range from visible to near IR. When the light is switched off, the transmittance bleaches back to its original state. So far, rare-earth (RE) including Y, Gd, Sc, Nd, Dy, Er, and Sm oxyhydride thin films have been discovered to exhibit the photochromic effect [2–7]. The tunable photochromic properties, adjustable bandgap, and the presence of photoconductivity make these photochromic films promising for applications in smart windows [7,8], memory devices [9], and photocatalysts [10].

However, the mechanism of the photochromic effect is still not fully clarified and a comprehensive understanding of the corresponding microstructural and electronic structure changes during photodarkening and bleaching is still lacking. By modelling optical spectroscopic ellipsometry data, Montero *et al.* [11] proposed that hydride-like metallic domains are formed in a semiconducting YH_xO_y matrix, with a volume fraction of up to 6% upon illumination. The formation of metallic domains was supported by a magnetic susceptibility study on Gd oxyhydride films in [12], where a reversible increase in the Curie-Weiss temperature for the photodarkened state was observed. In addition, a nuclear magnetic resonance study on RE oxyhydride films (RE = Sc) suggested that the photodarkening process is accompanied by a reduction of RE^{3+} to RE^{2+} [13]. Indeed, a previous

*Contact author: z.wu-2@tudelft.nl

positron annihilation study [14] showed (partially) reversible shifts in the positron Doppler-broadening S-W values in the direction towards the metal dihydride upon illumination in both YH_xO_y and GdH_xO_y films, suggesting the reversible formation of metallic nanodomains with a valence change from RE^{3+} to RE^{2+}. On the other hand, irreversible shifts in the S parameters to a higher value and the W parameters to a lower value after a photodarkening-bleaching cycle were also observed in both YH_xO_y and GdH_xO_y [14]. These irreversible shifts in the S parameters were found to correlate strongly with the bleaching time constant extracted from optical transmittance upon photodarkening-bleaching cycling, particularly for the first three cycles, suggesting that the microstructural changes corresponding to the slower bleaching upon cycling involve vacancy aggregation [15]. This was supported by PALS measurements before and after one cycle that suggests the irreversible formation of divacancy-like defects and growth of vacancy clusters as a result of the aggregation of light-induced hydrogen vacancies with the preexisting yttrium monovacancies and vacancy clusters [15]. The formation of vacancies is consistent with the observed release of hydrogen gas from YH_xO_y films during illumination, supporting the mobility of hydrogen liberated by the illumination [16]. However, it remains largely unknown how microstructure and electronic structure evolve in time during photodarkening and bleaching in RE oxyhydride films.

Positron annihilation lifetime spectroscopy (PALS) is a well-known nondestructive tool to identify and quantify open-volume defects at a nanometer-sized scale, providing information on the size and the concentration of open-volume defects. Because of the capability of relatively fast measurement (in the order of minutes), PALS has been employed to investigate vacancy dynamics in niobium during thermal annealing [17] and in hydrogen-charged nickel during aging at room temperature [18], and to examine the kinetics of vacancy clustering and precipitation during natural aging in Al-Mg-Si alloys [19–21]. It has also been applied to study the dynamic changes of the charge state of vacancy clusters after switching off the illumination in diamond [22]. In addition, our previous Doppler broadening positron annihilation spectroscopy (DB-PAS) study suggested that preferred positron trapping at metallic nanodomains occurs during illumination [14]. Indeed, if the positron affinity of the metallic nanodomains is different from the matrix, preferential positron trapping at nanometallic domains could occur, as has been observed in Li, Au, and Kr nanoclusters embedded in MgO [23–26], and in Cu nanoparticles embedded in Fe [27]. The preferential trapping at nanodomains could potentially increase the intensity of the corresponding positron lifetime component. For instance, in the Li-doped MgO system, the trapping rate and the intensity of positron annihilation at Li_2CO_3 precipitates increases almost linearly with the doping concentration of Li [28]. If the positron lifetime in a metallic domain is different from that of the surrounding matrix, the formation of metallic domains will change the positron lifetime. Therefore, PALS may provide essential information on the evolution of metallic domains and open-volume defects during photodarkening and bleaching.

In this study, we employed *in situ* illumination PALS measurements on two photochromic yttrium oxyhydride films to investigate (1) the time-evolution of the metallic domains and open-volume defects before illumination, during photodarkening and subsequent bleaching; and (2) the presence and nature of vacancy defects as a function of implantation energy (mean positron probe depth) before illumination and after bleaching. The PALS depth profiles show that there is no significant depth dependence of the vacancy defect distribution in the oxyhydride layer. The time-dependent PALS demonstrates a distinct behavior of the positron lifetime and intensity of each annihilation component in the PALS spectra during photodarkening and bleaching, providing key insights into the evolution of open-volume defects and metallic domains. This study deepens our understanding of the photochromism and the memory effect in yttrium oxyhydride films, and provides a method to study light-induced local structural changes at a nanometer scale and electronic changes in other photochromic polycrystalline films.

II. EXPERIMENTAL

Two types of yttrium dihydride thin films (YHO-1 and YHO-2) were deposited on unheated fused silica substrates ($1 \times 1\,cm^2$) by reactive magnetron sputtering in an Ar/H_2 (at a ratio of 7:1) atmosphere and the deposition pressure was maintained at 0.5 Pa during sputtering [2]. The dc power supplied to a yttrium target was 100 W and 200 W for YHO-1 and YHO-2 thin-film samples, respectively. The as-deposited yttrium dihydride thin films were then oxidized by exposure to an ambient environment. An oxyhydride phase was formed during the postoxidation process, in which at least five days were given to reach a stable composition [29]. The thickness of the oxyhydride layer in YHO-1 and YHO-2 samples was determined by profilometry to be 400 and 420 nm, with an uncertainty of ∼10%. The same deposition method as for the YHO-1 samples was used with a second yttrium target for preparing YHO-a film samples employed in the second PALS measurement at HZDR. The thickness of the oxyhydride layer in the YHO-a film samples was ∼350 nm.

Grazing-incidence x-ray diffraction (XRD) measurements were performed on a PANalytical X-pert Pro diffractometer with a Cu "Kα" source ($\lambda = 1.54$ Å) at room temperature at an angle of incidence of 2°. The XRD patterns of all yttrium oxyhydride films, compared with peak positions of reference *Fm*-3*m* YH_2 (#04–005–5940), are given in Fig. S1 within the Supplemental Material (SM) [30] (including Refs. [31–38]). The diffraction peaks of all yttrium oxyhydride films are consistent with the (shifted) positions of (111), (200) and (220) and (311) planes of the reference *Fm*-3*m* YH_2 (#04–005–5940), indicating that YHO-1, YHO-2, and YHO-a thin films have the same face-centered-cubic (fcc) crystal structure as YH_2. This is in agreement with previous findings [29]. Note that *Pnma* [39] and $P2_1/m$ [40] structures were reported in bulk YHO (in the 1:1:1 composition) and other crystal structures were reported in bulk RE oxyhydrides [40,41].

The optical transmittance of the yttrium oxyhydride film samples was measured in the wavelength range of 230–1120 nm using a custom-built optical fiber-based spectrometer [29]. A narrow band LED (385 nm, $I = 30\,mW/cm^2$) was employed as the light source to trigger the photochromic effect. The indirect optical bandgap energy of

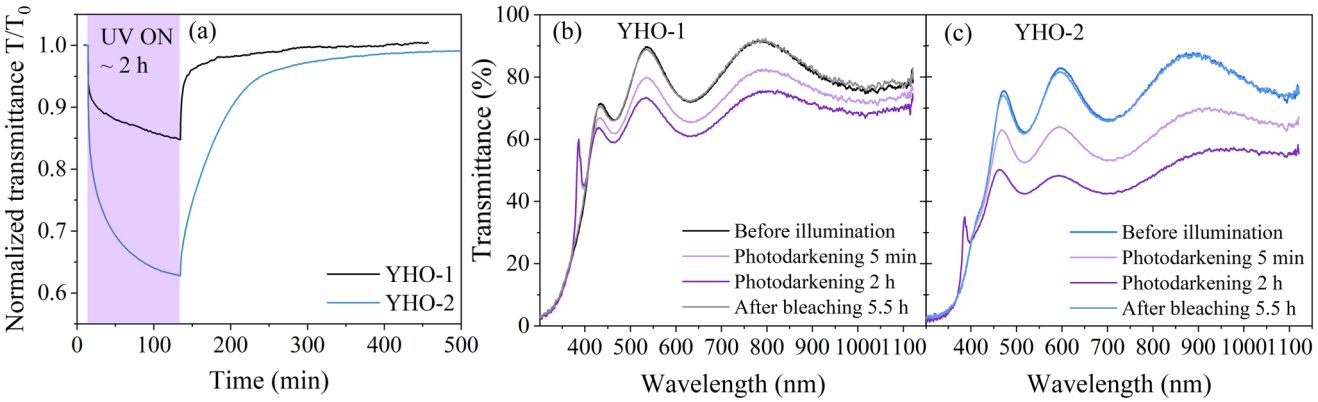

FIG. 1. (a) Optical transmittance normalized to the initial transmittance (T/T_0), averaged in the wavelength range of 450–1000 nm before illumination, during ~2 h ultraviolet (UV) illumination (purple-shaded region), and during subsequent bleaching for YHO-1 and YHO-2 thin-film samples. [(b),(c)] The corresponding transmittance spectra as a function of wavelength for the YHO-1 and YHO-2 thin-film samples before illumination, during 5 min and 2 h of photodarkening, and after 5.5 h of bleaching. Note that the transmittance peak around 380 nm seen during photodarkening is caused by the LED light source triggering the photochromic effect.

YHO-1, YHO-2, and YHO-a film samples was determined to be 2.49, 2.42, and 2.49 eV using a Tauc-plot method [29,42].

When implanted into a solid, a positron will collide with the atoms and lose its kinetic energy via electron excitations and interactions with the lattice. After a few picoseconds, the positron is thermalized with an energy of a few tens of meV. The thermalized positron diffuses through the host lattice until annihilation occurs in a defect-free environment or until it finds an open-volume defect. Open-volume defects such as negatively charged or neutral vacancies preferentially trap positrons owing to the lack of Coulomb repulsion of the ion cores. If the size of open-volume defects is sufficiently large, positronium, a bound state of a positron and an electron, can form. The positron lifetime depends on the local electron density at the annihilation site. The lifetime of a positron annihilating in the defect-free bulk state can vary from about 140 to 280 ps in semiconductors [43,44]. An increase in the size of open-volume defects will decrease the local electron density and thus increase the positron lifetime. The lifetime of orthopositronium (a bound state of an electron and a positron, with spin $S = 1$) in semiconductors is typically in the order of nanoseconds due to pick-off annihilation [44]. PALS can, therefore, be applied to examine the presence of open-volume defects and their size.

PALS measurements were performed at the Monoenergetic Positron Source (MePS) beamline, which is one of the end stations of the ELBE (Electron Linac for beams with high Brilliance and low Emittance) facility at Helmholtz-Zentrum Dresden-Rossendorf, Germany [45]. Approximately 10^7 counts were collected for each spectrum. Thanks to the high-flux low-energy positron beam, the acquisition time for one spectrum is about three minutes, enabling monitoring the microstructural changes at this time resolution. A $CeBr_3$ scintillator detector coupled to a Hamamatsu R13089-100 photomultiplier (PMT) tube was utilized for gamma quanta acquisition and the signals were processed by the SPDevices ADQ14DC-2X digitizer (14-bit vertical resolution and 2 GS/s horizontal resolution) [46]. The instrument time resolution was estimated to be ~250 ps by determination of the PALS spectrum of a reference amorphous yttria-stabilized zirconia (YSZ) sample with a single well-defined lifetime component. The positron lifetime spectra were analyzed by the convolution between the sum of N exponential decays $\sum_{i=1}^{N} \frac{I_i}{\tau_i} \exp(-t/\tau_i)$ and the time resolution function $R(t)$ of the spectrometer superimposed onto a constant background bkg, namely,

$$Z(t) = R(t) \otimes \sum_{i=1}^{N} \frac{I_i}{\tau_i} \exp(-t/\tau_i) + bkg,$$

where τ_i is the positron lifetime in state i and I_i is the corresponding intensity.

A three-component analysis was applied to decompose all positron lifetime spectra using the PALSfit3 program [47]. The average lifetime τ_{ave} is calculated as follows:

$$\tau_{ave} = \sum_{i=1}^{N} \tau_i I_i (i = 3), \quad I_1 + I_2 + I_3 = 1.$$

When the average lifetime exceeds the positron lifetime in the (defect-free) bulk material, it indicates the presence of open-volume defects. For the *in situ* illumination PALS measurements, an ultraviolet (UV) laser source (~375 nm) with a comparable intensity to the abovementioned LED was utilized. Using a custom-built beam expander consisting of three optical lenses, the diameter of the UV spot at the sample position was around 1.5 cm.

III. RESULTS AND DISCUSSION

A. Photochromic properties

The photochromic properties of YHO-1 and YHO-2 thin-film samples were examined by illuminating the film with UV light (3.2 eV) for 2 h. Figure 1(a) shows the transmittance T (averaged from 450 to 1000 nm) before illumination, during 2-h UV illumination (photodarkening), and the subsequent bleaching, normalized to the initial averaged transmittance T_0. The corresponding transmittance spectra as a function of

wavelength for the YHO-1 and YHO-2 thin-film samples before illumination, during 5 min and 2 h of photodarkening, and after 5.5 h of bleaching can be found in Figs. 1(b) and 1(c). For both yttrium oxyhydride thin-film samples, the transmittance reduces significantly during the first few minutes upon photodarkening and tends to stabilize with longer illumination time. The difference between the transmittance in virgin state T_0 and the transmittance at a time T, with respect to T_0, is defined as the photochromic contrast $(T_0 - T)/T_0$. After 2 h of UV illumination, the photochromic contrast reaches 15% and 37% for YHO-1 and YHO-2 samples, respectively. When the UV light is switched off, the transmittance starts to increase, and it can fully recover after bleaching for several hours. Comparing the two thin-film samples, a lower contrast and a faster bleaching rate were found for the YHO-1 sample. It is likely that, compared to the YHO-2 sample, the dihydride phase of the YHO-1 sample deposited at a lower deposition power has a higher porosity [48], enabling the absorption of more oxygen into the film during air oxidation, thus resulting in a higher O:H ratio in the YHO-1 sample. Indeed, the higher O:H ratio could explain the higher bandgap of the YHO-1 sample [29]. Furthermore, according to an ideal (model) face-center-cubic motif of yttrium oxyhydrides, the film with a higher O:H ratio has fewer hydrogen atoms at the octahedral sites [3], which is responsible for the lower contrast and faster bleaching of the YHO-1 sample [29,49], supposing that the release of octahedral hydrogen from its lattice position is a key factor for the photochromic effect.

B. *In situ* illumination positron lifetime experiments

In situ illumination PALS measurements were performed on YHO-1 and YHO-2 thin-film samples to investigate the evolution of open-volume defects and metallic domains during a photodarkening-bleaching cycle. Here, the UV illumination time for both samples is the same as in the transmittance measurements, i.e., 2 h. For the YHO-1 sample, the time monitoring the bleaching process is around 2.8 h, when the photodarkened film is nearly fully bleached. For the YHO-2 sample, the bleaching monitoring time for *in situ* PALS is 1.5 h, where photochromic contrast recovers by more than 80%.

1. PALS depth profiles before illumination and after photodarkening and bleaching

PALS depth profiles were collected in a positron implantation energy range from 0.5 up to 9 keV to monitor the open-volume defects as a function of positron implantation energy in YHO-1 and in YHO-2 thin-film samples before illumination and after bleaching. τ_{ave} is a robust parameter and rather insensitive to fitting procedures, leading to an accuracy within about 1 ps. Figures 2(a) and 2(b) show the average positron lifetime (τ_{ave}) as a function of positron implantation energy for both samples before illumination (grey squares), extracted from a three-component analysis of the positron lifetime spectra collected in PALS depth profiling measurements. Figure 2(a) also shows the τ_{ave} as a function of positron implantation energy after bleaching (red circles) for the YHO-1 sample, while in Fig. 2(b) the data point of τ_{ave} at 5 keV after bleaching (red circle) for the YHO-2 sample is shown for comparison, extracted from the time-dependent measurement performed at 5 keV (see Sec. III B 2).

Before illumination, the τ_{ave} values for both films are fairly constant in the range of 2–6 keV, while the values below 2 keV and above 6 keV are typically higher. Positrons with a higher energy can probe deeper into the materials. The positron implantation profiles in a material with density ρ in g/cm^3 are described by Makhovian implantation profiles,

$$P\,(z,\ E) = \frac{m z^{m-1}}{{z_0}^m} \exp\left[-\left(\frac{z}{z_0}\right)^m\right]$$

with $m = 2$, z the implantation depth, and $z_0 = 1.13\bar{z}$, with $\bar{z}$ the mean implantation depth in nm, is a function of the positron implantation energy E in keV according to $\bar{z}(E) = \frac{AE^n}{\rho}$, and we used $n = 1.6$ and $A = 4\,\mu\mathrm{g\,cm^{-2}\,keV^{-n}}$ [50,51], and $\rho = 4.3\,\mathrm{g/cm^3}$ for YH_xO_y, respectively.

As seen in Fig. 2(c), positrons at an implantation energy of about 6 keV starts to probe the region deeper than 400 nm. Hence, with increasing implantation energy above 6 keV, the increase in the average lifetime steadily results from the increased contribution from the substrate (>∼400 nm). This is consistent with the VEPFIT analysis of the DB-PAS depth profiles for the YHO-1 sample: Figure 2(d) shows that the derived fraction of positrons annihilating in the substrate layer starts to increase essentially above 6 keV. The fraction of positrons annihilating in each layer for the YHO-2 sample is similar to that for the YHO-1 sample (see Fig. S2 within the SM [30]). More details on the experimental DB-PAS depth profiles and the corresponding best-fit parameters for both samples can be found in Figs. S3 and S4 and Table SI (see the SM [30]). The higher τ_{ave} below 2 keV comes from the increased positron annihilation at the surface, which is supported by Fig. 2(d), which shows that the total fraction of positron annihilation from thermal and epithermal positrons increases with decreasing positron implantation energy below ∼2 keV. Therefore, the positron lifetimes in the range of 2–6 keV dominantly arise from the bulk oxyhydride layer. The τ_{ave} values above ∼360 ps of this bulk oxyhydride layer before illumination are much larger than the calculated and experimental defect-free bulk lifetime values of ∼240 ps reported in our previous studies, indicating the presence of open-volume defects [14,15] throughout the layer.

To provide more insights into the nature of open-volume defects in the samples before illumination, we continue here with a discussion of the lifetimes and intensities extracted from the three-component analysis of the respective positron lifetime spectra. Representative positron lifetime spectra collected at a positron implantation energy of 5 keV of YHO-1 and YHO-2 thin-film samples before illumination and the corresponding fits are shown in Fig. 3. The fairly constant τ_{ave} values in the range of 2–6 keV [Figs. 2(a) and 2(b)] as well as the corresponding positron lifetimes and intensities of the bulk oxyhydride layer (see Figs. S5 and S6 within the SM [30]) indicate that there is no significant depth dependence in the defect distribution in both samples. The depth dependence of the positron lifetimes and corresponding intensities obtained from a three-component analysis for YHO-1 and YHO-2 film samples in the collected positron implantation energy range can be found in Figs. S5 and S6 within the SM [30].

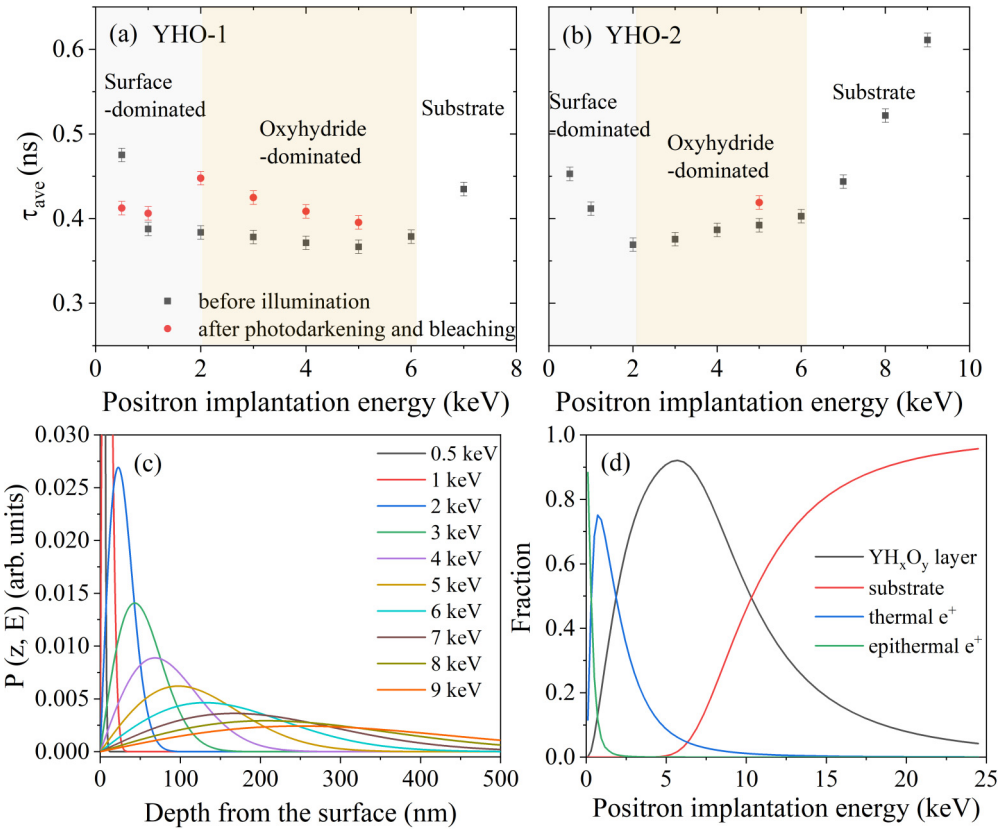

FIG. 2. The average positron lifetimes (τ_{ave}) as a function of positron implantation energy for (a) YHO-1 and (b) YHO-2 thin-film samples before illumination (grey squares) as well as after 2 h photodarkening and ∼2.8 h bleaching for the YHO-1 sample and ∼1.5 h bleaching for the YHO-2 sample (red circles), as well as (c) Makhovian positron implantation profiles for implantation energies from 0.5 keV to 9 keV for both YH_xO_y samples, and (d) the fractions of positrons annihilating in each layer for the YHO-1 film sample as a function of positron implantation energy derived by VEPFIT analysis.

The positron lifetimes and corresponding intensities of the three components averaged in the energy range of 3–5 keV for both YHO-1 and YHO-2 samples before illumination are shown in Table I.

The first shortest positron lifetime τ_1 of ∼277 ps is ∼13% larger than the experimental and calculated bulk lifetime values (∼240 ps) and is close to the calculated lifetime values for yttrium monovacancies (∼290 ps for LDA and ∼324 for GGA), so this first lifetime could be ascribed to yttrium monovacancies [14,15]. The corresponding intensity I_1 above 70% indicates that yttrium monovacancies are the dominant open-volume defects and positron trapping sites in both samples. The second lifetime in the range of 480–500 ps with an intermediate intensity (23–24%) arises from large vacancy

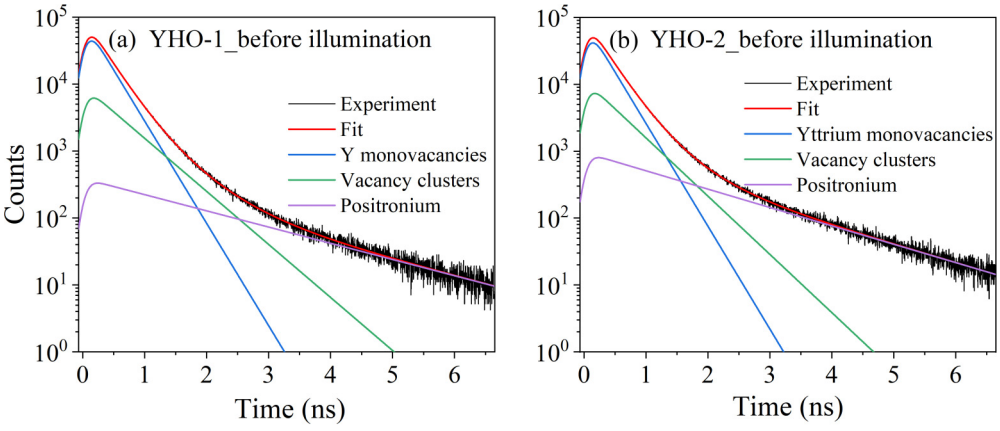

FIG. 3. Positron lifetime spectra collected at an implantation energy of 5 keV of (a) YHO-1 and (b) YHO-2 thin-film samples before illumination, and the corresponding three-component analyses. The background was fitted to be less than 1 for all fits.

TABLE I. Positron lifetimes (τ_i) and intensities (I_i) for the YHO-1 and YHO-2 thin-film samples before illumination, obtained from the average of the respective values extracted from the PALS spectra collected at 3–5 keV.

Sample	Status	τ_1 (ps)	τ_2 (ps)	τ_3 (ns)	I_1 (%)	I_2 (%)	I_3 (%)
YHO-1	before illumination	276 ± 2	498 ± 11	1.93 ± 0.04	74 ± 2	24 ± 1	2.7 ± 0.1
YHO-2	before illumination	277 ± 2	480 ± 15	1.54 ± 0.02	72 ± 2	23 ± 2	4.9 ± 0.1

clusters, and the size is likely larger than about five vacancies [14]. The longest positron lifetime values that are larger than ~1.5 ns indicate the formation of orthopositronium (o-Ps) in nanopores. The lifetime of o-Ps in vacuum is 142 ns, which can be reduced to a few nanoseconds by picking up and annihilating with one electron of opposite spin from the wall of the nanopore, which is known as the pick-off annihilation process [52–54]. Assuming a spherical shape, the averaged radius of pores can be estimated to be 0.29 nm and 0.25 nm in the oxyhydride layer of YHO-1 and YHO-2 samples using the Tao-Eldrup model [55,56]. These relatively large open-volume defects can be formed at grain boundaries and inside grains. The first and the second positron lifetimes of both films are larger than the reported experimental (~240 ps) and theoretical bulk lifetime of $YH_{2.5}O_{0.25}$ (~231 ps for LDA and ~241 for GGA) [15], and the sum of I_1 and I_2 is larger than 95%, indicating the presence of positron saturated trapping caused by a higher concentration of open-volume defects (typically $>\sim 10^{-4}$). Indeed, no reduced (first) bulk lifetime component was observed for these samples.

After 2 h photodarkening and fully bleaching, Fig. 2(a) shows that in the YHO-1 film sample τ_{ave} increases over a broad range of positron implantation energies from 2 to 5 keV, suggesting that the changes in open-volume defects occur throughout the whole oxyhydride layer. In addition, the increase in τ_{ave} at 5 keV in the YHO-2 sample is the same as the YHO-1 sample, i.e., about 27 ps. This is caused by an increase in the size and/or concentration of open-volume defects as a result of the photodarkening-bleaching cycle [15].

2. *Time-dependent positron lifetime experiments at 5 keV*

Time-dependent PALS measurements were performed at the selected implantation energy of 5 keV to investigate the evolution of microstructural and electronic structure changes during photodarkening and the subsequent bleaching. An implantation energy of 5 keV was selected, as at this implantation energy nearly all positrons are annihilating in the oxyhydride layer [Fig. 2(d)]. Figure 4 shows the τ_{ave} as a function of time before illumination, during photodarkening and bleaching in YHO-1 and YHO-2 thin-film samples. τ_{ave} is fairly constant for both samples before illumination, while it shows dynamic changes during photodarkening and bleaching. Upon photodarkening within the data collection time for one spectrum, i.e., ~3 min, τ_{ave} abruptly increases by 8 ps for the YHO-1 sample, while it decreases abruptly by 4 ps for the YHO-2 sample. The abrupt change in τ_{ave} indicates the occurrence of rapid microstructural and/or electronic structure changes, while the trend in τ_{ave} depends on the sample. During longer photodarkening, τ_{ave} changes slowly. Compared to the τ_{ave} at the beginning of photodarkening, τ_{ave} decreases by 1–2 ps after photodarkening of ~2 h. After the UV illumination is stopped, during bleaching τ_{ave} starts to increase significantly and tends to saturate on a time scale that is similar to that of the optical transmittance shown in Fig. 1. The similar time dependence of τ_{ave} to that of the transmittance during bleaching in both samples suggests that the increase in τ_{ave} during bleaching is related to the disappearance of the photodarkened state. The average lifetime τ_{ave} at the end of bleaching has increased by 25 ps and 27 ps for YHO-1 and YHO-2 samples compared to the values before illumination, which is consistent with the increments of τ_{ave} at 5 keV in depth profiling PALS measurements in Sec. III B 1. In addition, the stabilization of τ_{ave} at these increased values indicates that the light-induced microstructural changes after bleaching are rather stable.

In order to unravel the nature of microstructural changes and their evolution during photodarkening and bleaching, we now consider the time evolution of the three individual positron lifetimes and corresponding intensities from the three-component analysis. To reduce the statistical scattering in the fitting, I_2 was fixed to the averaged values either (1) before illumination or (2) during photodarkening and bleaching, as I_2 is nearly unchanged in these two time windows. The unfixed I_2 together with the positron lifetimes (τ_i) and other intensities (I_i) obtained from the fits after fixing I_2 are shown in Fig. 5 as a function of time before illumination, and during photodarkening and the subsequent bleaching for YHO-1 and YHO-2 thin-film samples at an implantation energy of 5 keV.

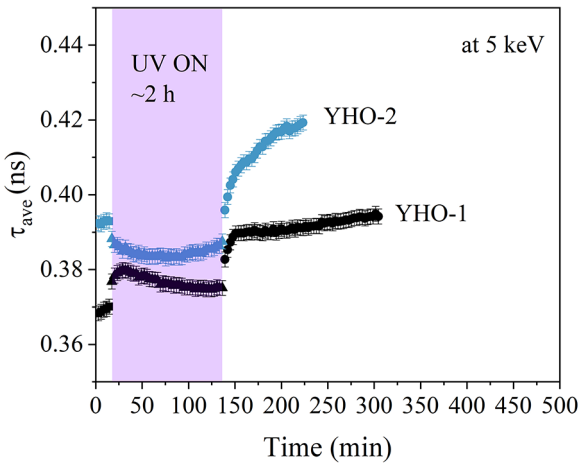

FIG. 4. Time dependence of the average positron lifetime (τ_{ave}) for YHO-1 and YHO-2 thin-film samples, extracted from the lifetime spectra collected at 5 keV during *in situ* illumination PALS measurements before illumination (squares), during photodarkening (~2 h, triangles, purple shaded area), and the subsequent bleaching (circles).

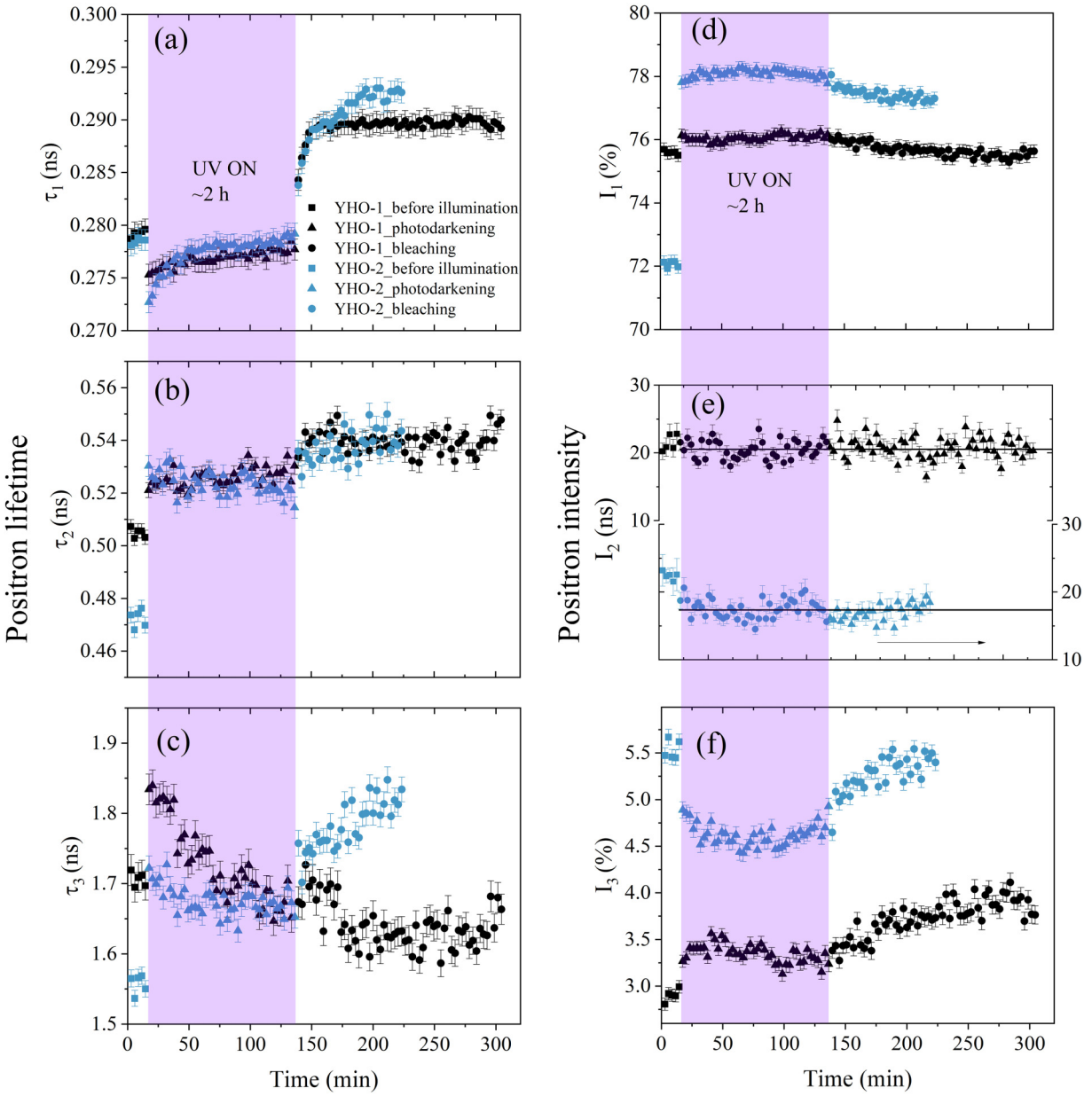

FIG. 5. Time dependence of the positron lifetimes (τ_i) and the corresponding intensities (I_i) extracted from the lifetime spectra collected at 5 keV during *in situ* illumination PALS measurements for both YHO-1 and YHO-2 thin-film samples before illumination (squares), during photodarkening (∼2 h, triangles, purple shaded area), and the subsequent bleaching (circles).

a. Time-evolution of the first positron lifetime component. As discussed in Sec. III B 1, before illumination the dominant shortest lifetime τ_1 of around 279 ps shown in Fig. 5(a) and Table II can be attributed to yttrium monovacancies. Upon photodarkening within ∼3 min, τ_1 abruptly drops by 4–6 ps. The lifetime parameters of the first PALS spectrum upon photodarkening reflect the average of the first 3 min, i.e., approximately the status of the film at around 1.5 min, as the first positron lifetime spectrum was collected in the period of 0–3 min after the UV light was switched on. The rapid drop in τ_1 may be related to the microstructural and electronic structure changes causing photodarkening, since the photochromic contrast initially reduces rapidly by more than 40% after illumination of 1.5 min for both samples, normalized to the total photochromic contrast reached after 2 h of photodarkening. A first possible cause of the rapid decrease in τ_1 can be the formation of metallic domains that was proposed to be the origin of the photochromic effect [11,14,57]. In previous *in situ* illumination DB-PAS studies, two types of metallic domains were proposed as possible alternative explanations for the photochromic effect, based on the reversible shifts in Doppler parameters and transmittance [14]. The first type involves the formation of phase-segregated hydrogen-rich metallic domains with a local composition of YH_2O_x ($x > 0.5$) in a mixed Y^{2+}/Y^{3+} valence state, caused by the local rearrangements of both hydrogen and oxygen

TABLE II. Positron lifetimes (τ_i) and intensities (I_i) for the YHO-1 and YHO-2 thin-film samples averaged from five PALS spectra before illumination, at the end of photodarkening, and at the end of bleaching, collected at 5 keV in the time-dependent PALS measurements.

Sample	Status	τ_1 (ps)	τ_2 (ps)	τ_3 (ns)	I_1 (%)	I_2 (%)	I_3 (%)
YHO-1	before illumination	279 ± 1	505 ± 2	1.71 ± 0.01	75.5 ± 0.2	22	2.9 ± 0.1
	at the end of illumination	278 ± 1	529 ± 2	1.67 ± 0.01	76 ± 0.2	21	3.3 ± 0.1
	after bleaching	290 ± 1	542 ± 2	1.64 ± 0.01	75.5 ± 0.2	21	3.9 ± 0.1
YHO-2	virgin state	278 ± 1	472 ± 2	1.56 ± 0.01	72 ± 0.2	22	5.5 ± 0.1
	at the end of illumination	279 ± 1	519 ± 2	1.68 ± 0.01	78 ± 0.2	17	4.7 ± 0.1
	after bleaching	293 ± 1	541 ± 2	1.82 ± 0.01	77 ± 0.2	17	5.4 ± 0.1

in the semiconducting oxyhydride matrix. For example, according to $2\ YH_2O_{0.5} \rightarrow YH_2O_{0.25} + YH_{1.5}O_{0.75} + 0.5\ H^0$, the resulting phase-segregated metallic $YH_2O_{0.25}$ has a mixed Y^{2+}/Y^{3+} valence, while the more H-poor $YH_{1.5}O_{0.75}$ retains the Y^{3+} valence. This is similar to what has been reported in a spectroscopic ellipsometry study [11], where the ellipsometry data under illumination are successfully modelled by the formation of yttrium hydride-like metallic domains in a semiconducting matrix, and 2% of such metallic domains could explain a reduction in transmittance of ∼30%. Additionally, the change in the valence state of Y is further supported by a recent NMR study that demonstrates a clear Knight shift of Sc NMR resonance for part of the Sc cations upon photodarkening, which is attributed to the change in electron shielding caused by the formation of metallic domains, suggesting a reduction of RE^{3+} to RE^{2+} upon photodarkening [7,13]. We furthermore note that the calculated positron bulk lifetime of $YH_{1.9}$ is 225 ps and 229 ps in the framework of LDA and GGA, and the experimental bulk lifetime of $YH_{1.9}$ of ∼260 ps is also smaller than the value before illumination (279 ps) [14]. More details on *ab initio* calculation methods can be found within the SM [30]. If hydride-like metallic domains are formed and trap positrons upon photodarkening, a reduction in τ_1 as observed in the first ∼3 min would therefore indeed be expected. The second type of metallic domains proposed are formed by a hydrogen vacancies-induced Anderson-Mott insulator-to-metal transition, which was inspired by the well-known insulator-to-metal transition from yttrium trihydrides to dihydrides [14,58]. In this scenario, electron-hole pairs are generated under illumination. Subsequently, some of the H^- anions at the octahedral sites capture a photoexcited hole and form H^0 atoms ($H^- + h^+ \rightarrow H^0$), which become mobile and leave their lattice positions, while some of the photoexcited electrons may localize at Y ($4d$) orbitals around the positively charged hydrogen vacancies owing to charge compensation. When the concentration of such Y ($4d$) electrons at the octahedral sites is sufficiently large, these electron orbitals start to overlap and form an electron band. Compared to the phase-segregated H-rich metallic domains, the formation of hydrogen vacancies-induced metallic domains is more easily achieved chemically since it only requires the removal of hydrogen from octahedral sites, for instance, according to $2\ YH_2O_{0.5} \rightarrow 2YH_{1.75}O_{0.5} + 0.5\ H^0$. Therefore, we believe that the second type of metallic domains are formed rather than the first type, in line with what was previously concluded in ref. [7]. The formed positively charged hydrogen vacancies essentially will not influence the positron lifetime as they repel positrons. However, the formation of electron bands in metallic domains caused by the overlapping of electron orbitals at Y $4d$ around hydrogen vacancies will significantly increase the electron density locally. This may cause a decrease in the shortest lifetime if part of positrons annihilate at those metallic domains. Note that the positron lifetime associated with annihilation in such Anderson-Mott type of metallic domains is unknown, and would require further *ab initio* calculations to gain insights into its exact value. Overall, the formation of metallic domains may well explain the abrupt drop of τ_1 and the substantial reduction of transmittance.

An alternative explanation for the sudden decrease in τ_1 may consist of a change in the charge state of monovacancies caused by the capturing of photoexcited electrons, e.g., from V^+ to V^0. A transition of the charge state of vacancies was previously observed in the photon-illuminated GaN [59], diamond [22], GaAs [60,61], *n*-type SiC [62], and Si [63] systems. For example, the study on GaAs showed that the positron lifetime of the photoinduced negatively charged As monovacancies V_{As} is 28 ps smaller than that of the respective neutral vacancies in GaAs, caused by the strong inward relaxation of the gallium atoms neighboring negatively charged V_{As} vacancies compared to the neutral vacancies, leading to an increase in electron density at the vacancies [60]. A previous study showed that the as-prepared Gd oxyhydride films are *p*-type semiconductors, and the hole density is on the order of $\sim 10^{11}$–$10^{12}\ cm^{-3}$, indicating a mild doping level [64]. Assuming a similar case for Y oxyhydride films, the *p*-type character of the film will lead to a position of the Fermi level close to the valence band maximum, and part of yttrium monovacancies might capture holes and turn into a charge-neutral state V_Y^0. Upon photodarkening, the *n*-type characteristic become dominant [64], and neutral yttrium monovacancies could easily capture a photoexcited electron and become negatively charged ($V_Y^0 + e^- \rightarrow V_Y^-$). This transition in charge state and the associated inward relaxation of neighboring atoms may lead to a fast reduction of τ_1 in YH_xO_y. We further note that, in some cases, it was observed that the change of charge state of vacancy defects in GaN [59], diamond [22], 6H-SiC [60], and Si [63] significantly affects the trapping rate rather than the lifetime of the respective defects. Therefore, the transition from V_Y^0 to V_Y^- might explain the increase in I_1 as well as the reduction in τ_1. Note, however, that the extent of the possible presence of V_Y^0 is not determined in the as-prepared YH_xO_y films, and possibly occurring changes in the charge state of Y monovacancies would need further detailed investigation, for instance, of the involved vacancy formation energies and determination of the position of the Fermi energy level of the as-deposited films and during

photodarkening. A second option of the change in the charge state of vacancies that could occur in YH_xO_y upon photodarkening would be from V_H^+ to V_H^0 or V_H^-. The positively charged anion vacancies cannot trap positrons but the neutral or negatively charged anion vacancies might trap positrons. For instance, the neutral As vacancies and O vacancies have been detected by PAS in GaAs and $LaSrCoO_3$, respectively [60,65]. Therefore, V_H^0 or V_H^- might trap positrons, but the positron lifetime at such vacancies is unknown. Further investigations on the charge state of vacancies would need temperature-dependent PALS measurements [63,66–68] and/or theoretical *ab initio* positron lifetime calculations. Note here that in this case, there would be a competition between the change in the charge state of hydrogen vacancies by capturing photoexcited electrons and the localization of electrons at Y ($4d$) orbitals around hydrogen vacancies as suggested by the Anderson-Mott insulator-to-metal related mechanism. This could be unravelled by calculating the binding energy of electrons with hydrogen vacancies and at Y ($4d$) orbitals.

During further photodarkening, in contrast to the initial abrupt drop, τ_1 increases gradually for at least the first 30 min, after which it tends to stabilize at 278–279 ps. It is expected that in this timeframe additional metallic domains are gradually formed, leading to the further decrease in transmittance. If more trapping of positrons at metallic domains occurs, one would expect a continual decrease in τ_1. However, the increase in τ_1 suggests the occurrence of an additional microstructural change, for instance, the formation of divacancies. Namely, under photodarkening, some of the hydrogen vacancies created by UV illumination could aggregate with the preexisting yttrium monovacancies and form divacancies $V_Y{-}V_H$ or small vacancy complexes consisting of V_Y and a few neighboring hydrogen vacancies when the hydrogen vacancies are creating in the vicinity of an yttrium monovacancy. The gradual increase in τ_1 during further photodarkening indicates increased positron trapping at such divacancy-like defects owing to an increase in the concentration of those defects that are continuously created by the UV illumination. At the end of photodarkening, τ_1 tends to stabilize in parallel with the transmittance, which implies that positron trapping at the divacancy-like defects, preexisting yttrium monovacancies, metallic domains, and possibly at charged cation and/or anion monovacancies in the semiconducting YH_xO_y matrix reaches an equilibrium state in the presence of UV illumination because of the stabilization of the light-induced microstructural and electronic structure changes.

After the UV illumination was stopped, τ_1 during bleaching increases on a time scale similar to the increase in the optical transmittance until it stabilizes at ∼289 ps for the YHO-1 sample and at ∼293 ps for the YHO-2 sample. At the end of bleaching, the transmittance is largely recovered as a result of the disappearance of metallic domains, meaning that the high τ_1 values of ∼289 ps and ∼293 ps at the end of bleaching can be attributed to the light-induced formation of divacancy-like defects or small vacancy complexes in the YH_xO_y semiconductor. Noticeably, compared to the value before illumination, τ_1 after bleaching has increased by ∼4% and 5% for YHO-1 and YHO-2 samples. This is smaller than the typical increment in lifetime (>10%) from monovacancies to divacancies in Si, GaAs, and 6H-SiC [69,70], and suggests that only part of the yttrium monovacancies are transformed into divacancies or small vacancy complexes [15]. The larger increase in τ_1 in the YHO-2 sample compared with the YHO-1 sample could be caused by the formation of more divacancy-like defects due to the larger photochromic contrast, suggesting that more microstructural changes take place during illumination for this more H-rich sample.

b. Correlation of the first positron lifetime component with photochromic contrast during bleaching. During bleaching, the gradual increase in τ_1 for both samples is understandable, since the decrease in positron trapping at metallic domains (and possibly at charged monovacancies) because of the gradual disappearance of the metallic domains and photogenerated charge carriers will lead to an increase in positron trapping at the preexisting yttrium monovacancies and at the illumination-induced divacancy-like defects, and increase τ_1. Noteworthy, the time dependence of both τ_{ave} and τ_1 during bleaching [Figs. 4 and 5(a)] is similar to the photochromic contrast (Fig. 1). The time evolution of the photochromic contrast during bleaching is shown in Fig. 6(a), while the correlation diagrams of τ_{ave} and τ_1 versus the photochromic contrast in YHO-1 and YHO-2 thin-film samples during bleaching are plotted in Figs. 6(b)–6(e). Clearly, for both samples, during the initial period of ∼15 min in the bleaching phase, τ_{ave} and τ_1 increase almost linearly with decreasing photochromic contrast. Quantitatively, during this period, τ_1 increases by 11 ps with an decrease in photochromic contrast of 11% in the YHO-1 sample, while in sample YHO-2 the increase in τ_1 and the decrease in photochromic contrast are 10 ps and 11%. This strong correlation between τ_1 and the photochromic contrast in these two samples suggests that the quantity of metallic domains that disappear during this first fast bleaching phase (I) and the correspondingly increased fraction of positron trapping at yttrium monovacancies and divacancy-like defects are quantitatively very similar in both samples. During further bleaching, τ_1 for the YHO-1 sample tends to stabilize at around 289 ps when the contrast still decreases ∼4%. It is likely that during this second bleaching phase (II) in the YHO-1 sample, positron saturation trapping at yttrium monovacancies and divacancy-like defects occurs while the positron trapping at metallic domains is tiny owing to the small concentration and/or size of metallic domains (resulting in a small contrast ∼4%), so the disappearance of metallic domains does not noticeably increase the positron trapping at yttrium monovacancies and divacancy-like defects, resulting in a relatively stable τ_1. However, during further bleaching in the YHO-2 sample, τ_1 increases further by 4 ps with decrease in contrast of ∼20%. The second correlation between τ_1 and the photochromic contrast during this second bleaching phase (II) in the YHO-2 sample indicates a continued decrease in positron trapping at metallic domains owing to the disappearance of metallic domains and correspondingly increased positron trapping at yttrium monovacancies and divacancy-like defects, but with slower kinetics. The fact that after 2 h of photodarkening a much higher contrast in the YHO-2 sample is reached as compared to the YHO-1 sample suggests that more and possibly larger metallic domains are formed in sample YHO-2. Indeed, if larger metallic domains are formed in the YHO-2 sample, the disappearance of larger metallic domains would require

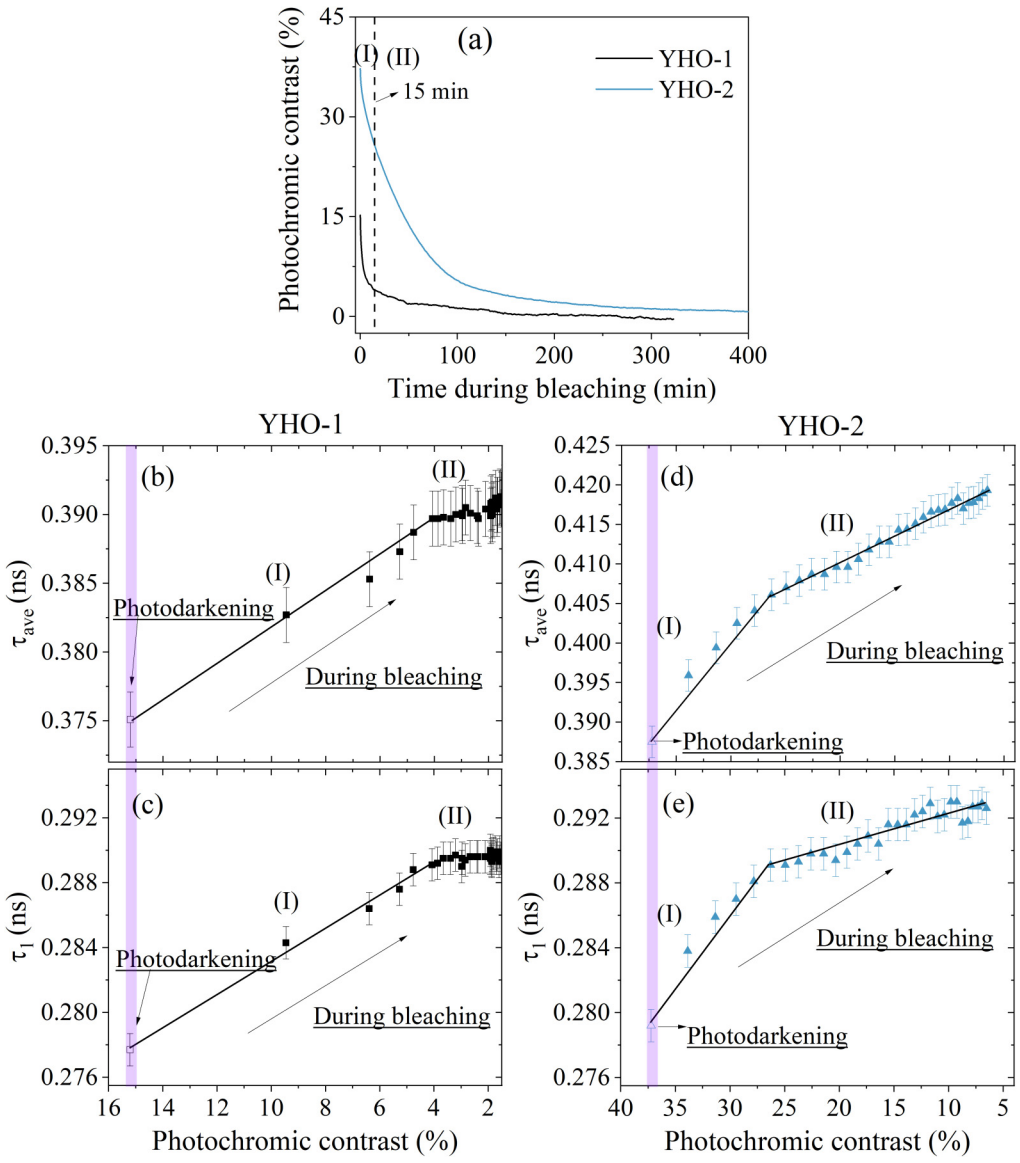

FIG. 6. Photochromic contrast as a function of time during bleaching (a), as well as the relationship between τ_{ave} respectively τ_1 with the photochromic contrast in YHO-1 [(b),(c)] and YHO-2 [(d),(e)] thin-film samples at the end of photodarkening and during bleaching. The solid lines are a guide for the eyes, with bleaching phase (I) corresponding to the first ∼15 min of bleaching for both samples and bleaching phase (II) corresponding to the time interval after ∼15 min of bleaching.

longer bleaching time owing to the longer diffusion distance of hydrogen anions [15,71]. Therefore, the slower increase in τ_1 with decreasing photochromic contrast during the second bleaching phase (II) in the YHO-2 sample could be caused by the slower disappearance of those metallic domains that are originally large in size, while the similar first bleaching phase (I) may correspond to the disappearance of metallic domains that are smaller in size.

c. Time evolution of the second and third positron lifetime components. For the second lifetime τ_2, the value before illumination of around 470 and 500 ps in Fig. 5(b) and Table II arises from vacancy clusters (V_n, $n \geqslant 5$). Upon photodarkening for the first ∼3 min, the observed fast increase in τ_2 to ∼520–530 ps could be a consequence of fast release of loosely bounded hydrogen atoms from the walls of the vacancy clusters and/or hydrogen molecules from the vacancy clusters [14,15]. Indeed, Moldarev *et al.* showed that the partial hydrogen pressure reaches the highest value during the first ∼5 min of UV illumination of a photochromic YH_xO_y film, suggesting the presence of a fast process of hydrogen release [16]. During illumination for longer times, τ_2 hardly changes, while during bleaching it increases up to about 540 ps within ∼20 min (the YHO-1 smple) to ∼40 min (the YHO-2 sample). The increase in lifetime during bleaching indicates the detection of vacancies with a larger size. However, vacancy formation and aggregation are likely to occur only during illumination, when the photogenerated charge carriers liberate hydrogen and create hydrogen vacancies. Therefore, it is possible that during photodarkening, the light-induced anion vacancies aggregate with the preexisting vacancy clusters and form larger open-volume defects, similar to the formation of divacancy-like defects from the yttrium monovacancies.

Vacancy formation and aggregation would induce an increase in the positron lifetime; however, τ_2 is fairly constant during photodarkening. The unchanged τ_2 suggests the presence of other processes during photodarkening that can reduce τ_2 and compensate for the increase. If some metallic domains are formed in the vicinity of vacancy clusters, τ_2 can be reduced owing to the locally increased electron density. In addition, the increased concentration of photoexcited electrons in the semiconducting matrix might increase the electron density around vacancy clusters as well and reduce τ_2. During bleaching, metallic domains at the boundaries of vacancy clusters and photoexcited electrons in the semiconducting matrix gradually disappear, leading to a gradual decrease in the electron density around the grown vacancy clusters, and thus causing a gradual increase in τ_2 on a timescale that is quite similar to that of the optical transmittance [Fig. 6(a)]. The τ_2 values of ∼540 ps at the end of the bleaching phase for both samples suggest a similar size of the grown vacancy clusters after the photodarkening-bleaching cycle, which is consistent with the results in the previous PALS study [15].

The third positron lifetime τ_3 is fairly constant before illumination, and the value of above ∼1.5 ns [Fig. 5(c)] is an indication of formation of orthopositronium in nanopores. Upon photodarkening for the first 3 min, τ_3 rises abruptly by ∼8% up to 1.84 ns for the YHO-1 sample and by 10% up to 1.71 ns for the YHO-2 sample. The increase in τ_3 of 8–10% could be the result of an increased size of nanopores because of the release of hydrogen molecules from these nanopores [16]. During photodarkening, τ_3 reduces at least in the first 30 minutes owing to the formation of metallic areas near the surface of nanopores (leading to faster pick-off annihilation) and tends to stabilize, while during bleaching it varies from sample to sample.

d. Time variation of positron trapping rates/intensities. Because of the presence of positron saturated trapping at open-volume defects in the films, the concentration of the defects cannot be determined. However, the changes of I_1 and I_2 during photodarkening and bleaching could reflect the changes in the corresponding positron trapping rates κ_1 and κ_2 at the sites associated with τ_1 and τ_2, while I_3 reflects the probability of forming o-Ps at a formation rate κ_3, which undergo pick-off annihilation in nanopores.

In the YHO-1 sample, upon photodarkening for the first ∼3 min, both I_1 and I_3 increase about 0.5% (Fig. 5), while I_2 decreases ∼1% accordingly ($I_1 + I_2 + I_3 = 1$). Upon photodarkening, based on the abrupt increase in the positron lifetime for vacancy clusters τ_2 (V_n, $n \geqslant 5$) owing to the release of hydrogen, one would expect an increase in the corresponding trapping rate κ_2, via an increase in the trapping coefficient [44]. However, the decrease in I_2 and the increase in I_1 and I_3 in the YHO-1 sample upon photodarkening for the first ∼3 min indicates that the relative fraction of positrons trapping at the vacancy clusters decreases owing to the larger increase in κ_1 and κ_3 compared to κ_2. Indeed, the formed metallic domains could act as new trapping sites and enhance the trapping rate κ_1, in line with the previous DB-PAS study that showed preferential positron trapping at metallic domains [14]. Furthermore, if some monovacancies are charged by the photoexcited electrons upon photodarkening, the trapping rate κ_1 could also be increased by the enhanced attractive Coulomb force for positrons. Indeed, it was reported that the intensity of the positron lifetime associated with the $V_{Ga}(V_N)_n$ defects (n = 2−4) nearly doubles in GaN under illumination [59], which was assigned to the increase in the trapping rate owing to the change in the charge state of vacancies by capturing photoexcited electrons. In addition, the aggregation of light-induced hydrogen vacancies with yttrium monovacancies may already appear at small concentrations, which could increase κ_1 as well via increasing the trapping coefficient compared to the one for monovacancies [44]. Therefore, upon photodarkening for the first ∼3 min, the occurrence of new and more effective trapping sites leads to an increase in κ_1 in the YHO-1 sample. On the other hand, the abrupt increase in I_3 ($\Delta I_3 \cong +0.5\%$) in the YHO-1 sample indicates an enhanced probability of forming o-Ps, which could be caused by hydrogen release from the nanopores. If some nanopores of comparable size contain hydrogen molecules before illumination, upon illumination the release of those hydrogen molecules could make the previously invisible nanopores detectable via o-Ps formation, thereby increasing I_3.

For the YHO-2 sample, upon photodarkening for the first 3 min, both I_2 and I_3 decreases, while only I_1 increases. Upon photodarkening for the first 3 min, similar to the YHO-1 sample, the release of hydrogen from vacancy clusters and some nanopores that contain hydrogen molecules before illumination could also occur in sample YHO-2, which could potentially increase the positron trapping rate at vacancy clusters κ_2 and the probability of forming o-Ps I_3. Nevertheless, the relatively large increase in I_1 ($\Delta I_1 \cong +6\%$) leads to a net reduction in both I_2 and I_3 in the YHO-2 sample. This indicates that upon photodarkening for the first 3 min, the relative positron trapping rate at vacancy clusters κ_2/κ_1 and the relative probability of forming o-Ps κ_3/κ_1 decrease, caused by the larger, more dominate increase in the positron trapping rate κ_1 at the annihilation sites associated with τ_1. As discussed, the formation of metallic domains and divacancies, as well as the change in the charge state of monovacancies could increase κ_1 and I_1. Compared to the YHO-1 sample, the larger increase in κ_1 and I_1 in the YHO-2 sample could be owing to more changes in microstructure and electronic structure upon photodarkening for the first 3 min. Indeed, the photochromic contrast after 1.5 min of UV illumination in sample YHO-2 is about twice that in the YHO-1 sample, indicating that more metallic domains are formed in this more H-rich YHO-2 sample. Also, more hydrogen vacancies will be formed with increasing concentration of metallic domains, which leads to an increase in the probability of forming divacancy-like defects and the corresponding trapping rate κ_1.

During further photodarkening, I_1, I_2, and I_3 for both samples remain nearly unchanged, indicating that positron trapping rates at the sites associated with τ_1 and τ_2, and the probability of forming o-Ps remain balanced. During bleaching, for both samples, I_2 continues to remain nearly unchanged, while I_1 decreases and I_3 increases slightly over the whole bleaching period. The correlation between τ_1 and the photochromic contrast during bleaching suggests that little or no positron trapping occurs at metallic domains anymore after 15 min in sample YHO-1. Therefore, the gradual changes in I_3 and I_1 during bleaching cannot be (solely) attributed to the reduced trapping at the independent metallic domains

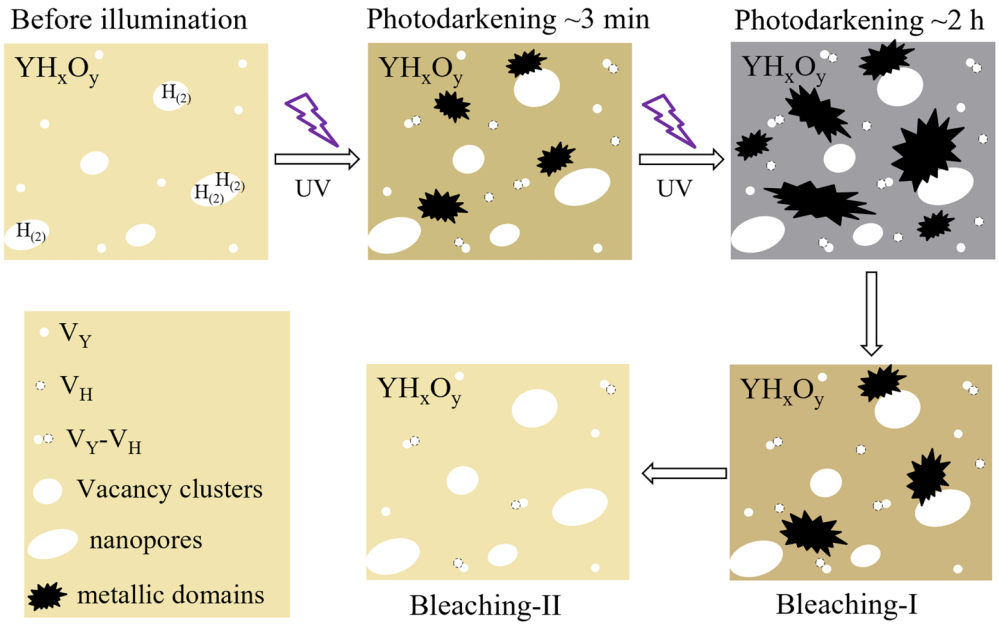

FIG. 7. Schematics of the evolution of open-volume defects and metallic domains along with a corresponding change in film color before illumination, during photodarkening, and subsequent two bleaching phases in photochromic yttrium oxyhydride films.

in the semiconducting matrix owing to the disappearance of those metallic domains. However, the increase in I_3 indicates that the probability of forming o-Ps increases. This could be the result of a decrease in the metallicity around nanopores, as it is well known that a metallic environment is less effective in converting positron to positronium, compared to porous metal oxide insulators and semiconductors that can efficiently generate positronium [72,73].

In general, our *in situ* illumination PALS experiments provide key insights into the evolution of open-volume defects and metallic domains in time as well as the correlation with optical transmittance during photodarkening-bleaching processes. The dynamics of open-volume defects and metallic domains along with a corresponding change in film color before illumination, during photodarkening for the first ~3 min and photodarkening ~2 h, and subsequent two bleaching phases (I and II) in yttrium oxyhydride films is schematically sketched in Fig. 7.

3. Second PALS experiment

Our previous DB-PAS study [15] on both YH_xO_y and GdH_xO_y thin-film samples under multiple photodarkening-bleaching cycles demonstrated that the S parameter after bleaching increases progressively upon cycling for the first three cycles and correlates with an increasingly slower bleaching rate. Combined with the results of PALS measurements before and after one cycle, this correlation suggests that the microstructural changes corresponding to the slower bleaching involve vacancy aggregation owing to the release of hydrogen [15]. Indeed, both the depth-profile and time-dependent measurements show a significant increase in τ_{ave} for both YHO-1 and YHO-2 samples after the photodarkening-bleaching cycle (Figs. 2 and 4), which is consistent with results in [15]. However, direct experimental evidence from positron lifetime spectroscopy on vacancy formation/aggregation upon photodarkening-bleaching cycling is important to gain more insights into the changes in open-volume defects upon multiple photochromic cycling. We therefore performed PALS measurements on an additional sample YHO-a, deposited the same way as the YHO-1 sample, during three photodarkening-bleaching cycles in a second PALS experiment at HZDR, in which each cycle included a short illumination time of ~9 min. The statistical scattering and the minor changes in positron lifetime parameters made it difficult in this case to discern the separate changes in the positron lifetime parameters for the three individual components after each cycle. Therefore, we present in Fig. 8 the robust τ_{ave} parameter collected at 4 keV as a function of time for the YHO-a sample during the three photodarkening-bleaching cycles. The positron implantation energy chosen in these time-dependent measurements for sample YHO-a was 4 keV, since the thickness of this film (~350 nm) was slightly less than the that of the YHO-1 sample. Note that the bleaching monitoring times during the first and second cycles used in this experiment were sufficient to fully bleach the sample for the applied illumination time of ~9 min (see Fig. 9 for the corresponding time dependence of the optical transmittance).

Figure 8 shows that the average positron lifetime τ_{ave} of the YHO-a sample increases progressively during these three photodarkening-bleaching cycles, which is in line with the increase in τ_{ave} in YHO-1 and YHO-2 samples after one cycle (Fig. 4) and also with the successive increase in the S parameter upon multiple cycling reported in [15], suggesting that more and/or larger nanoscale open-volume defects are formed upon cycling. In addition, we notice that the increase in τ_{ave} after the first cycle (4 ps) is larger than the increments of τ_{ave} after bleaching for the following two cycles (about 3 ps in total). This is consistent with the behavior of the S parameter upon photochromic cycling, that reveal that the

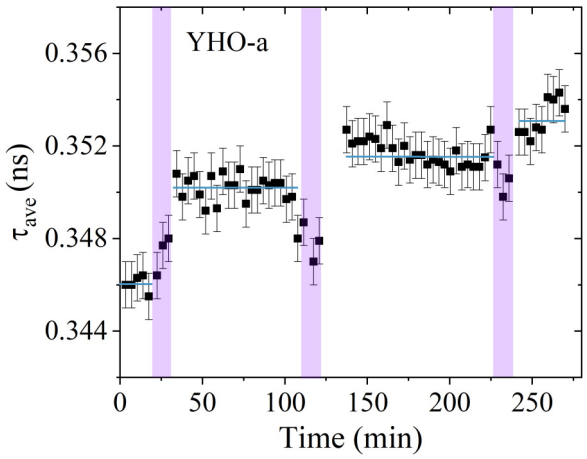

FIG. 8. Time dependence of the average positron lifetime (τ_{ave}) for the YHO-a sample, extracted from the lifetime spectra collected at 4 keV during *in situ* illumination PALS measurements before illumination and during three short photodarkening (∼9 min, purple-shaded area)-bleaching cycles.

increase in the S parameter after the first cycle is larger than the following two cycles in YH_xO_y films [15], suggesting that the changes in the open-volume defects are the largest for the first cycle. Indeed, the loosely bonded hydrogen atoms and/or nonbonded hydrogen molecules in vacancy clusters and nanopores preferentially seem to be released during the first photodarkening [16], causing the largest change in τ_{ave} and the S parameter after the first cycle. Furthermore, compared to the increase in τ_{ave} in YHO-1 and YHO-2 samples after photodarkening (2 h) and the subsequent bleaching of 25–27 ps as shown in Fig. 4, the much smaller increments in the YHO-a sample after each photodarkening-bleaching cycle (2–4 ps) is likely related to the formation of fewer hydrogen vacancies due to the substantially shorter illumination time, leading to a lower probability of formation of vacancy complexes.

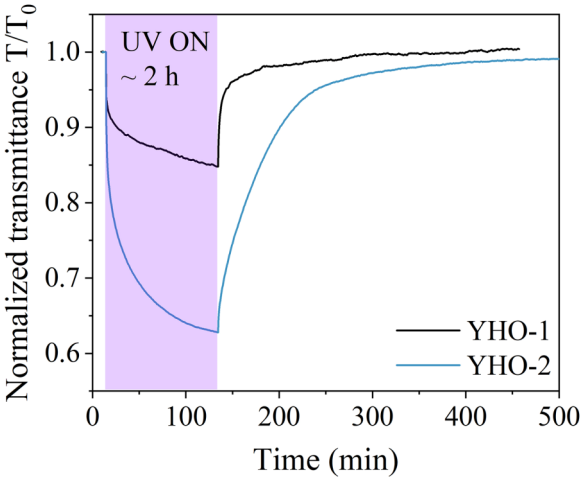

FIG. 9. Optical transmittance normalized to the initial transmittance (T/T_0), averaged in the wavelength range of 450–1000 nm for sample YHO-a during three short photodarkening (∼9 min, purple-shaded region)-bleaching cycles.

IV. CONCLUSIONS

In this study, yttrium oxyhydride thin-film samples deposited at two different sputtering power were investigated. The PALS depth profiles show that there is no significant depth dependence in the distribution of open-volume defects in the bulk oxyhydride layer for both samples. After photodarkening and subsequent bleaching, the homogeneous increase in τ_{ave} in the range of 2–5 keV suggests that an increase in the size/concentration of open-volume defects occurs throughout the whole oxyhydride layer.

In situ illumination PALS measurements at 5 keV revealed the time evolution of open-volume defects and metallic domains of the oxyhydride layer for both YHO-1 and YHO-2 thin-film samples during photodarkening-bleaching processes. Upon photodarkening for the first 3 min, for both samples a sudden drop in the shortest positron lifetime τ_1 and a significant reduction in transmittance is observed, that results from the fast initial formation of metallic domains. In parallel, the occurrence of the sudden increase in τ_2 and τ_3 suggests the release of loosely bounded hydrogen from vacancy clusters and nanopores. During further photodarkening, the gradual increase in τ_1 suggests that the concentration of divacancy-like defects in the semiconducting matrix increases. When the UV illumination is switched off, two subsequent bleaching phases are observed. During the first bleaching phase (I), a linear relationship between τ_1 and the photochromic contrast is seen that is quantitatively similar for both samples, suggesting that the quantity of metallic domains that disappear during the first bleaching phase, and the correspondingly increased positron trapping at yttrium monovacancies and divacancy-like defects is similar in both samples. During the second bleaching phase (II), metallic domains continue to disappear, but the remaining small size or concentration of metallic domains prevents their detection by PALS in the YHO-1 sample with a small photochromic contrast (>4%), as indicated by a relatively stable τ_1. In contrast, in the more H-rich sample YHO-2 a second linear relationship between τ_1 and the photochromic contrast is observed during the bleaching phase II, which could be caused by the disappearance of those metallic domains that have grown larger during photodarkening. After bleaching, most of the metallic domains and the photoexcited charge carriers in the semiconducting matrix have disappeared, while the grown open-volume defects remain stable. This study deepens our understanding of the (nanoscale) structure-optical property relationship in photochromic yttrium oxyhydrides.

ACKNOWLEDGMENTS

The authors thank the facility staff at ELBE at the Helmholtz-Zentrum Dresden-Rossendorf e.V., a member of the Helmholtz Association, for their assistance in the positron lifetime experiments. Z.W. thanks Prof. Dr. Morten Eldrup from Technical University of Denmark for providing a license key of the PALSfit3 program. This research was financially supported by Guangzhou Elite Project and the Materials for Sustainability programme (Grant No. 680.M4SF.034) of the Dutch Research Council (NWO).

[1] T. Mongstad, C. Platzer-Bjorkman, J. P. Maehlen, L. P. A. Mooij, Y. Pivak, B. Dam, E. S. Marstein, B. C. Hauback, and S. Z. Karazhanov, A new thin film photochromic material: Oxygen-containing yttrium hydride, Sol. Energy Mater. Sol. Cells **95**, 3596 (2011).

[2] F. Nafezarefi, H. Schreuders, B. Dam, and S. Cornelius, Photochromism of rare-earth metal-oxy-hydrides, Appl. Phys. Lett. **111**, 103903 (2017).

[3] S. Cornelius, G. Colombi, F. Nafezarefi, H. Schreuders, R. Heller, F. Munnik, and B. Dam, Oxyhydride nature of rare-earth-based photochromic thin films, J. Phys. Chem. Lett. **10**, 1342 (2019).

[4] S. M. Adalsteinsson, M. V. Moro, D. Moldarev, S. Droulias, M. Wolff, and D. Primetzhofer, Correlating chemical composition and optical properties of photochromic rare-earth oxyhydrides using ion beam analysis, Nucl. Instrum. Meth. B **485**, 36 (2020).

[5] D. Chaykina, F. Nafezarefi, G. Colombi, S. Cornelius, L. J. Bannenberg, H. Schreuders, and B. Dam, Influence of crystal structure, encapsulation, and annealing on photochromism in Nd oxyhydride thin films, J. Phys. Chem. C **126**, 2276 (2022).

[6] D. Chaykina, G. Colombi, H. Schreuders, and B. Dam, Photochromic samarium oxyhydride thin films, AIP Adv. **13**, 055211 (2023).

[7] B. Dam, F. Nafezarefi, D. Chaykina, G. Colombi, Z. Wu, S. W. H. Eijt, S. Banerjee, G. A. de Wijs, and A. Kentgens, Perspective on the photochromic and photoconductive properties of rare-earth oxyhydride thin films, Sol. Energy Mater. Sol. Cells **273**, 112921 (2024).

[8] Y. J. Ke, J. W. Chen, C. J. Lin, S. C. Wang, Y. Zhou, J. Yin, P. S. Lee, and Y. Long, Smart windows: Electro-, thermo-, mechano-, photochromics, and beyond, Adv. Energy Mater. **9**, 1902066 (2019).

[9] T. Yamasaki, R. Takaoka, S. Iimura, J. Kim, H. Hiramatsu, and H. Hosono, Characteristic resistive switching of rare-earth oxyhydrides by hydride ion insertion and extraction, Acs Appl. Mater. Inter. **14**, 19766 (2022).

[10] L. Andronic, D. Moldarev, D. Deribew, E. Moons, and S. Z. Karazhanov, Photocatalytic self-cleaning properties of thin films of photochromic yttrium oxyhydride, J. Solid State Chem. **316**, 123599 (2022).

[11] J. Montero, F. A. Martinsen, M. Garcia-Tecedor, S. Z. Karazhanov, D. Maestre, B. Hauback, and E. S. Marstein, Photochromic mechanism in oxygen-containing yttrium hydride thin films: An optical perspective, Phys. Rev. B **95**, 201301(R) (2017).

[12] J. Montero, P. Svedlindh, and L. Österlund, Photo-induced reversible modification of the Curie-Weiss temperature in paramagnetic gadolinium compounds, Solid State Commun. **378**, 115419 (2024).

[13] S. Banerjee, D. Chaykina, G. Colombi, B. Dam, G. A. de Wijs, and A. P. M. Kentgens, Studying photochromism in scandium oxyhydrides: Solid-state NMR studies and DFT calculations, (unpublished).

[14] Z. Wu, T. de Krom, G. Colombi, D. Chaykina, G. van Hattem, H. Schut, M. Dickmann, W. Egger, C. Hugenschmidt, E. Brück, B. Dam, and S. W. H. Eijt, Formation of vacancies and metallic-like domains in photochromic rare-earth oxyhydride thin films studied by *in-situ* illumination positron annihilation spectroscopy, Phys. Rev. Mater. **6**, 065201 (2022).

[15] Z. Wu, L. de Wit, M. Beek, G. Colombi, D. Chaykina, H. Schreuder, H. Schut, M. O. Liedke, M. Butterling, A. Wagner, M. Dickmann, E. Brück, B. Dam, and S. W. H. Eijt, The memory effect in photochromic rare-earth oxyhydride thin films studied by in-situ positron annihilation spectroscopy upon photodarkening-bleaching cycling, Phys. Rev. Mater. **8**, 045201 (2024).

[16] D. Moldarev, L. Stolz, M. V. Moro, S. M. Adalsteinsson, I. A. Chioar, S. Z. Karazhanov, D. Primetzhofer, and M. Wolff, Environmental dependence of the photochromic effect of oxygen-containing rare-earth metal hydrides, J. Appl. Phys. **129**, 153101 (2021).

[17] M. Wenskat, J. Čižek, M. Oskar Liedke, M. Butterling, M. Stiehl, G. Dalla Lana Semione, C. Backes, C. Bate, O. Melikhova, E. Hirschmann, A. Wagner, H. Weise, A. Stierle, M. Aeschlimann, and W. Hillert, Vacancy dynamics in niobium and its native oxides and their potential implications for quantum computing and superconducting accelerators, Phys. Rev. B **106**, 094516 (2022).

[18] L. Chiari, K. Kojima, Y. Endo, H. Teshigahara, M. Butterling, M. Oskar Liedke, E. Hirschmann, A. G. Attallah, A. Wagner, and M. Fujinami, Formation and time dynamics of hydrogen-induced vacancies in nickel, Acta Mater. **219**, 117264 (2021).

[19] J. Banhart, M. D. H. Lay, C. S. T. Chang, and A. J. Hill, Kinetics of natural aging in Al-Mg-Si alloys studied by positron annihilation lifetime spectroscopy, Phys. Rev. B **83**, 014101 (2011).

[20] M. Liu, J. Cizek, C. S. T. Chang, and J. Banhart, Early stages of solute clustering in an Al-Mg-Si alloy, Acta Mater. **91**, 355 (2015).

[21] M. Madanat, M. Liu, and J. Banhart, Reversion of natural ageing in Al-Mg-Si alloys, Acta Mater. **159**, 163 (2018).

[22] J. M. Mäki, F. Tuomisto, A. Varpula, D. Fisher, R. U. A. Khan, and P. M. Martineau, Time dependence of charge transfer processes in diamond studied with positrons, Phys. Rev. Lett. **107**, 217403 (2011).

[23] M. A. van Huis, A. van Veen, H. Schut, C. V. Falub, S. W. H. Eijt, P. E. Mijnarends, and J. Kuriplach, Positron confinement in embedded lithium nanoclusters, Phys. Rev. B **65**, 085416 (2002).

[24] C. V. Falub, P. E. Mijnarends, S. W. H. Eijt, M. A. van Huis, A. van Veen, and H. Schut, Electronic structure and orientation relationship of Li nanoclusters embedded in MgO studied by depth-selective positron annihilation two-dimensional angular correlation, Phys. Rev. B **66**, 075426 (2002).

[25] J. Xu, J. Moxom, B. Somieski, C. W. White, A. P. Mills, R. Suzuki, and S. Ishibashi, Positronic probe of vacancy defects on surfaces of Au nanoparticles embedded in MgO, Phys. Rev. B **64**, 113404 (2001).

[26] M. A. van Huis, A. van Veen, H. Schut, B. J. Kooi, and J. T. M. De Hosson, Formation of solid Kr nanoclusters in MgO, Phys. Rev. B **67**, 235409 (2003).

[27] Y. Nagai, T. Chiba, Z. Tang, T. Akahane, T. Kanai, M. Hasegawa, M. Takenaka, and E. Kuramoto, Fermi surface of nanocrystalline embedded particles in materials: Bcc Cu in Fe, Phys. Rev. Lett. **87**, 176402 (2001).

[28] G. H. Dai, Q. J. Yan, Y. Wang, and Q. S. Liu, Li-doped MgO as catalysts for oxidative coupling of methane—A positron-annihilation study, Chem. Phys. **155**, 275 (1991).

[29] G. Colombi, T. De Krom, D. Chaykina, S. Cornelius, S. W. H. Eijt, and B. Dam, Influence of cation (RE = Sc, Y, Gd) and O/H anion ratio on the photochromic properties of REO_xH_{3-2x} thin films, Acs Photonics **8**, 709 (2021).

[30] See Supplemental Material at http://link.aps.org/supplemental/10.1103/PhysRevMaterials.9.015201 for x-ray diffraction patterns, the fraction of positrons annihilating in each layer as a function of implantation energy for the YHO-2 sample, DB-PAS depth profiles and the corresponding best-fit parameters, the positron lifetimes and the corresponding intensities as a function of positron implantation energy, and positron lifetime calculation methods.

[31] H. Schut, A variable energy positron beam facility with applications in materials science, Ph.D. thesis, Delft University of Technology, Delft, 1990.

[32] A. van Veen, H. Schut, J. Devries, R. A. Hakvoort, and M. R. Ijpma, Analysis of positron profiling data by means of VEPFIT, AIP Conf. Proc. **218**, 171 (1990).

[33] M. Torrent, F. Jollet, F. Bottin, G. Zérah, and X. Gonze, Implementation of the projector augmented-wave method in the ABINIT code: Application to the study of iron under pressure, Comput. Mater. Sci. **42**, 337 (2008).

[34] B. Barbiellini, M. J. Puska, T. Torsti, and R. M. Nieminen, Gradient correction for positron states in solids, Phys. Rev. B **51**, 7341 (1995).

[35] N. A. W. Holzwarth, A. R. Tackett, and G. E. Matthews, A projector augmented wave (PAW) code for electronic structure calculations, Part I: Atompaw for generating atom-centered functions, Comput. Phys. Commun. **135**, 329 (2001).

[36] S. Goedecker, M. Teter, and J. Hutter, Separable dual-space gaussian pseudopotentials, Phys. Rev. B **54**, 1703 (1996).

[37] E. Boronski and R. M. Nieminen, Electron-positron density-functional theory, Phys. Rev. B **34**, 3820 (1986).

[38] J. P. Perdew, K. Burke, and M. Ernzerhof, Generalized gradient approximation made simple, Phys. Rev. Lett. **77**, 3865 (1996).

[39] N. Zapp, H. Auer, and H. Kohlmann, YHO, an air-stable ionic hydride, Inorg. Chem. **58**, 14635 (2019).

[40] K. Fukui, S. Iimura, J. Wang, T. Tada, T. Honda, K. Ikeda, T. Otomo, and H. Hosono, Stabilization factor of anion-excess fluorite phase for fast anion conduction, Chem. Mater. **33**, 1867 (2021).

[41] K. Fukui, S. Iimura, T. Tada, S. Fujitsu, M. Sasase, H. Tamatsukuri, T. Honda, K. Ikeda, T. Otomo, and H. Hosono, Characteristic fast H^- ion conduction in oxygen-substituted lanthanum hydride, Nat. Commun. **10**, 2578 (2019).

[42] J. Tauc, R. Grigorovici, and A. Vancu, Optical properties and electronic structure of amorphous germanium, Phys. Status Solidi. **15**, 627 (1966).

[43] B. Barbiellini, P. Genoud, and T. Jarlborg, Calculation of positron lifetimes in bulk materials, J. Phys. Condens. Mat. **3**, 7631 (1991).

[44] R. Krause-Rehberg and H. S. Leipner, *Positron Annihilation in Semiconductors–Defect Studies*, (Springer-Verlag, Berlin, 1999).

[45] A. Wagner, M. Butterling, M. O. Liedke, K. Potzger, and R. Krause-Rehberg, Positron annihilation lifetime and doppler broadening spectroscopy at the ELBE facility, AIP Conf. Proc. **1970**, 040003 (2018).

[46] E. Hirschmann, M. Butterling, U. H. Acosta, M. O. Liedke, A. G. Attallah, P. Petring, M. Görler, R. Krause-Rehberg, and A. Wagner, A new system for real-time data acquisition and pulse parameterization for digital positron annihilation lifetime spectrometers with high repetition rates, J. Instrum. **16**, P08001 (2021).

[47] J. V. Olsen, P. Kirkegaard, and M. Eldrup, Analysis of positron lifetime spectra using the PALS*fit*3 program, AIP Conf. Proc. **2182**, 040005 (2019).

[48] K. Eufinger, D. Poelman, H. Poelman, R. De Gryse, and G. B. Marin, Photocatalytic activity of dc magnetron sputter deposited amorphous TiO_2 thin films, Appl. Surf. Sci. **254**, 148 (2007).

[49] D. Chaykina, I. Usman, G. Colombi, H. Schreuders, B. Tyburska-Pueschel, Z. Wu, S. W. H. Eijt, L. J. Bannenberg, G. A. de Wijs, and B. Dam, Aliovalent calcium doping of yttrium oxyhydride thin films and implications for photochromism, J. Phys. Chem. C **126**, 14742 (2022).

[50] V. J. Ghosh, Positron implantation profiles in elemental and multilayer systems, Appl. Surf. Sci. **85**, 187 (1995).

[51] A. Zubiaga, J. A. Garcia, F. Plazaola, F. Tuomisto, J. Zuniga-Perez, and V. Munoz-Sanjose, Positron annihilation spectroscopy for the determination of thickness and defect profile in thin semiconductor layers, Phys. Rev. B **75**, 205305 (2007).

[52] W. Brandt, S. Berko, and W. W. Walker, Positronium decay in molecular substances, Phys. Rev. **120**, 1289 (1960).

[53] R. S. Vallery, P. W. Zitzewitz, and D. W. Gidley, Resolution of the orthopositronium-lifetime puzzle, Phys. Rev. Lett. **90**, 203402 (2003).

[54] C. Hugenschmidt, Positrons in surface physics, Surf. Sci. Rep. **71**, 547 (2016).

[55] S. J. Tao, Positronium annihilation in molecular substances, J. Chem. Phys. **56**, 5499 (1972).

[56] M. Eldrup, D. Lightbody, and J. N. Sherwood, The temperature-dependence of positron lifetimes in solid pivalic acid, Chem. Phys. **63**, 51 (1981).

[57] D. Chaykina, T. de Krom, G. Colombi, H. Schreuders, A. Suter, T. Prokscha, B. Dam, and S. Eijt, Structural properties and anion dynamics of yttrium dihydride and photochromic oxyhydride thin films examined by *in situ* μ^+ SR, Phys. Rev. B **103**, 224106 (2021).

[58] K. K. Ng, F. C. Zhang, V. I. Anisimov, and T. M. Rice, Electronic structure of lanthanum hydrides with switchable optical properties, Phys. Rev. Lett. **78**, 1311 (1997).

[59] A. Uedono, T. Tanaka, N. Ito, K. Nakahara, W. Egger, C. Hugenschmidt, S. Ishibashi, and M. Sumiya, Electron capture by vacancy-type defects in carbon-doped GaN studied using monoenergetic positron beams, Thin. Solid. Films **639**, 78 (2017).

[60] K. Saarinen, P. Hautojarvi, P. Lanki, and C. Corbel, Ionization levels of As vacancies in as-grown GaAs studied by positron-lifetime spectroscopy, Phys. Rev. B **44**, 10585 (1991).

[61] S. Kuisma, K. Saarinen, P. Hautojarvi, C. Corbel, and C. LeBerre, Optical processes related to arsenic vacancies in semi-insulating GaAs studied by positron spectroscopy, Phys. Rev. B **53**, 9814 (1996).

[62] S. Arpiainen, K. Saarinen, P. Hautojärvi, L. Henry, M. F. Barthe, and C. Corbel, Optical transitions of the silicon vacancy in 6H-SiC studied by positron annihilation spectroscopy, Phys. Rev. B **66**, 075206 (2002).

[63] H. Kauppinen, C. Corbel, J. Nissila, K. Saarinen, and P. Hautojarvi, Photoionization of the silicon divacancy studied by positron-annihilation spectroscopy, Phys. Rev. B **57**, 12911 (1998).

[64] G. Colombi, B. Boshuizen, D. Chaykina, L. Y. Hsu, H. Schreuders, T. J. Savenije, and B. Dam, Large polaron conduction, photoconductivity, and photochromism in GdH_xO_{3-2x} oxyhydride thin films, Adv. Opt. Mater. **11**, 2202660 (2023).

[65] T. Friessnegg, S. Madhukar, B. Nielsen, A. R. Moodenbaugh, S. Aggarwal, D. J. Keeble, E. H. Poindexter, P. Mascher, and R. Ramesh, Metal ion and oxygen vacancies in bulk and thin film $La_xSr_{1-x}CoO_3$, Phys. Rev. B **59**, 13365 (1999).

[66] M. J. Puska and R. M. Nieminen, Theory of positrons in solids and on solid-surfaces, Rev. Mod. Phys. **66**, 841 (1994).

[67] D. J. Keeble, S. Singh, R. A. Mackie, M. Morozov, S. McGuire, and D. Damjanovic, Cation vacancies in ferroelectric $PbTiO_3$ and $Pb(Zr, Ti)O_3$: A positron annihilation lifetime spectroscopy study, Phys. Rev. B **76**, 144109 (2007).

[68] J. Mahony and P. Mascher, Positron-annihilation study of vacancy defects in InAs, Phys. Rev. B **55**, 9637 (1997).

[69] P. Hautojarvi, Defects in semiconductors - recent progress in positron experiments, Mater. Sci. Forum **175**, 47 (1995).

[70] L. Henry, M. F. Barthe, C. Corbel, P. Desgardin, G. Blondiaux, S. Arpiainen, and L. Liszkay, Silicon vacancy-type defects in as-received and 12-MeV proton-irradiated 6H-SiC studied by positron annihilation spectroscopy, Phys Rev B. **67**, 115210 (2003).

[71] J. Crank, *The Mathematics of Diffusion*, 2nd ed. (Oxford University Press, London, 1975).

[72] D. B. Cassidy and A. P. Mills, The production of molecular positronium, Nature (London) **449**, 195 (2007).

[73] B. S. Cooper, A. M. Alonso, A. Deller, L. Liszkay, and D. B. Cassidy, Positronium production in cryogenic environments, Phys. Rev. B **93**, 125305 (2016).